Footprint Study of Ultrasonic Wedge-Bonding with Aluminum Wire on Copper Substrate

I. LUM,[1,2] M. MAYER,[1] and Y. ZHOU[1]

1.—Microjoining Laboratory, Center for Advanced Materials Joining, Department of Mechanical Engineering, University of Waterloo, Waterloo, ON, Canada N2L 3G1. 2.—E-mail: ilum@engmail.uwaterloo.ca

The effects of the process parameters of ultrasonic power and normal bonding force on bond formation at ambient temperatures have been investigated with scanning electron microscopy (SEM) and energy-dispersive x-ray (EDX) analysis. A model was developed based on classical microslip theory[1] to explain the general phenomena observed in the evolution of bond footprints left on the substrate. Modifications to the model are made due to the inherent differences in geometry between ball-bonding and wedge-bonding. Classical microslip theory describes circular contacts undergoing elastic deformation. It is shown in this work that a similar microslip phenomenon occurs for elliptical wire-to-flat contacts with plastically deformed wire. It is shown that relative motion exists at the bonding interface as peripheral microslip at lower powers, transitioning into gross sliding at higher powers. With increased normal bonding forces, the transition point into gross sliding occurs at higher ultrasonic bonding powers. These results indicate that the bonding mechanisms in aluminum wire wedge-bonding are very similar to those of gold ball-bonding, both on copper substrate. In ultrasonic wedge-bonding onto copper substrates, the ultrasonic energy is essential in forming bonding by creating relative interfacial motion, which removes the surface oxides.

Key words: Wire-bonding mechanism, copper substrates, aluminum wire, ultrasonic power, friction, wear

INTRODUCTION

Wire-bonding is the most utilized method for making electrical interconnections from an integrated circuit (IC) to a substrate. Annually, more than 4 trillion wire-bonds are made.[2] The flexibility and cost effectiveness of wire-bonding make it widely accepted in industry. Among the variations of wire-bonding techniques, the predominant method used today is thermosonic ball-bonding of gold wire onto aluminum metallization, but there are many applications for another method called ultrasonic wedge-bonding. For instance, in interconnecting power devices, ultrasonic wedge-bonding of large diameter aluminum wires is the preferred method[2] due to its low material cost. Another advantage of aluminum wire wedge-bonding is that the bonds on aluminum pads are more reliable than those with gold wire. Ultrasonic wedge-bonding uses a normal bond force simultaneously with ultrasonic energy to form the first and second bonds and, with aluminum wire, is usually performed at ambient temperatures. However, despite being both widely accepted in industry and an older technology than ball-bonding,[2] there is a lack of an understanding of the bonding mechanisms,[2,3,4] compared to recent work in ball-bonding.[5]

Aluminum is the typical metallization used for ICs. Recently, the industry is moving toward using copper metallization,[6,7] since it possesses better electrical properties than aluminum such as lower electrical resistance.[6] However, the oxide that forms on copper is more tenacious than that on aluminum and hence causes difficulties during wire bonding,[2] which may result in poor bond strength. Although an oxide layer also forms on aluminum, it does not pose a large problem for bonding since it is brittle and easily breaks up and is dispersed.[2] Researchers have shown that it is possible to produce reliable ultrasonic wedge-bonds on copper with aluminum wire at room temperature.[8]

Currently, low-k materials are becoming more common as insulation layers;[9,10] however, these materials

(Received March 18, 2005; accepted October 5, 2005)

are lacking the mechanical stability to survive the wire-bonding process. In order to use the wire-bonding process on low-k materials, damage to the low-k material would need to be prevented and low stress wire-bonding may be a solution. An improved process understanding for wedge-bonding will help to meet such current challenges.

This study focuses on the role of process parameters in the ultrasonic wedge-bonding of aluminum wire on copper substrate at ambient temperatures. The bond footprints left on the substrate were examined with scanning electron microscopy (SEM) for microwelded regions and changes in the morphology of the substrate surface. A model for wedge-bonding is reported and compared with an existing model for ball-bonding.

Technical Background

Wire-bonding using typical process settings is generally accepted to be a solid-state joining process,[11] which is supported by various evidence such as bonds made at liquid nitrogen temperatures[12] and studies of the bond interface with transmission electron microscopy.[13] A major requirement to form a metallurgical bond is a relatively contaminant-free surface. Without occurrence of melting in the wire-bonding process, other methods of contaminant dispersal are required in order to facilitate bonding.

Deformation is the main mechanism responsible for the contaminant dispersal required for bond formation in thermocompression (using heat and pressure only) wire-bonding.[14] The deformation mechanism observed in thermocompression bonding is similarly observed in pressure welding, in which applied pressure and the subsequent deformation breaks up the oxide layer.[15] In ultrasonic wire-bonding, ultrasonic energy is used in addition to pressure. When a metal is irradiated with ultrasonic energy, the yield stress decreases, and this is known as the reversible ultrasonic softening effect.[16] According to some authors, the ultrasonic energy only acts to increase the amount of deformation.[4,12] However, this view was shown to be incomplete, as Zhou et al.[17] reported that bonds made with and without ultrasonic energy but possessing the same amount of deformation showed different amounts of bonding and strength. Clearly, this result shows that ultrasonic energy contributes to ultrasonic bonding in a way other than by increased deformation alone. The additional effect of ultrasonic energy may be the creation of relative motion between the wire and substrate, as inferred by Mayer[18] using in-situ microsensors. Mayer showed that relative motion at the ball/substrate interface was important in bond formation; when no sliding occurred, there was no bonding at ambient temperature.

The dynamic force supplied by the ultrasonic transducer during bonding causes the bonding tip and hence the wire/substrate faying interface to move in a reciprocating manner with the amplitude of the bonding tip oscillation being proportional to the ultrasonic power applied.[19] The relative motion that occurs at the faying interface will lead to wear of material or contaminant similar to that described by an equation developed for other contacting surfaces in relative motion (adapted from Ref. 20):

$$d = t \times \frac{KPV}{H} \tag{1}$$

where d is the depth of wear, t is the time in relative motion, K is the wear coefficient constant, P is the mean pressure, V is the sliding velocity, and H is the hardness of the material for which the depth of wear is being calculated. A typical application of Eq. 1 is for calculating wear in bearings. In ultrasonic bonding, V is a function of ultrasonic power, frequency, and compliance. This wear of material is termed "fretting" when small oscillations are involved. A relatively clean surface is necessary for bonding to occur, and the wear of material by relative motion can result in the required surface cleanliness. For wire-bonds, d therefore is assumed to correlate with the amount of bonding.

In ultrasonic wire-bonding, the bonding tool applies a bonding force and ultrasonic vibration to the wire/substrate combination, which may be simplified as a contact pair under both normal and tangential forces. Mindlin[1] studied the compliance of two perfectly elastic spheres subjected to combined normal force, N, and tangential force, S. When the spheres are brought into contact with a normal force N, the contact area is over a circle of radius a, and is proportional to $N^{1/3}$. Macroscopic gross sliding initiates when the tangential force exceeds a critical value, $\mu_s N$, where μ_s is the coefficient of static friction. However, with application of a tangential force less than the critical value, a shear traction q is introduced over the contact area. It was shown that the traction would rise to infinity at the periphery if no slip occurred. Obviously, an infinite traction stress is not attainable, and therefore, in order to relieve the stress, the contacting material at the periphery will have to undergo slip, and under this condition is termed "microslip."

An equation was provided by Mindlin[1] to calculate the size of the microslip region (Fig. 1a):

$$a' = a\left(1 - \frac{S}{\mu_s N}\right)^{1/3} \tag{2}$$

where a′ is the annulus inner radius, a is the contact radius, and $S \leq \mu_s N$. In Fig. 1, the ultrasound-bonding force parameter space is illustrated. The ultrasonic force is mainly directed tangentially to the interface. There exists a separate regime of microslip and a separate regime of gross sliding demarcated by a transition line termed "line of friction" in Ref. 21. The slope of this line is proportional to μ_s. Microslip and gross sliding exist below and above the transition line, respectively. Illustration A in Fig. 1 shows that in the microslip regime, microslip occurs at an annulus, $a' < r < a$, on the contact zone, while no slip occurs within the circle of radius a′, i.e., the stationary region. As shown by

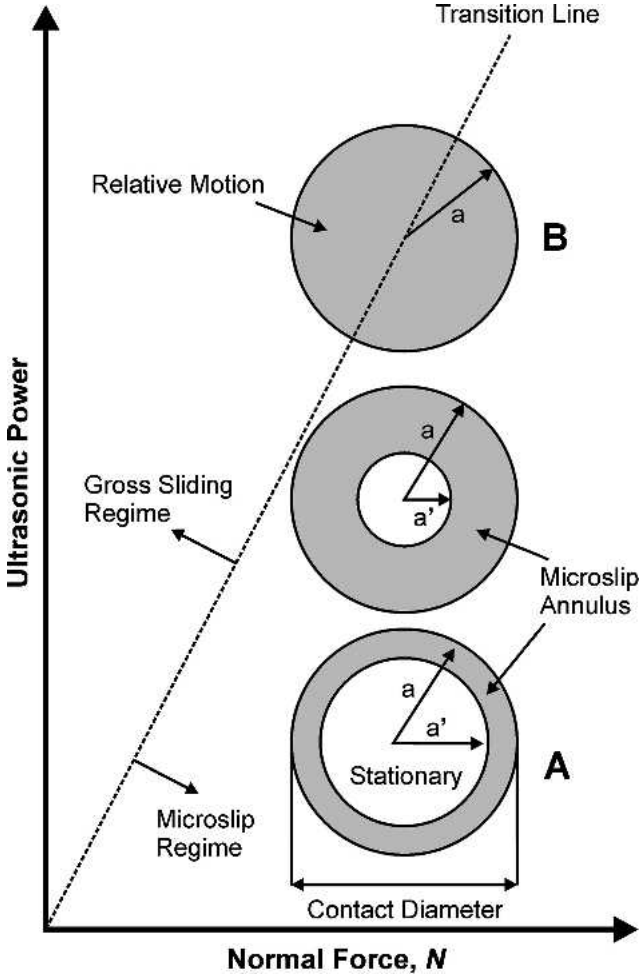

Fig. 1. Schematic illustration of (A) stationary and microslip regions in a circular contact undergoing microslip and (B) circular contact showing area undergoing relative motion on the verge of gross sliding (a′ = 0).

Eq. 2, the microslip annulus inner radius decreases with increasing tangential force up to the point of gross sliding (i.e., $S = \mu_s N$) at which time the microslip annulus inner radius has decreased to the center of the contact circle and vanished, as shown by illustration B in Fig. 1.

Johnson[22] studied the effect of oscillating tangential forces on the surface of a metal plate in contact with a metal sphere and the evidence lends support to Mindlin's microslip theory.[1] It was shown by Johnson that at low applied tangential forces, before the onset of gross sliding, a fretted annulus due to microslip was observed on the surface of the plate. As the magnitude of the tangential force was increased, the annulus inner radius moved inward until it reached the center on the verge of gross sliding. A similar phenomenon was observed by Lum et al.[5] in their study of ultrasonic gold ball-bonding. A transition from microslip to gross sliding with increasing ultrasonic energy (tangential force) was observed in the ball-bond. However, the authors are not aware of reports on observations of similar phenomena in wedge-bonding.

EXPERIMENTAL METHODS

25-μm-diameter aluminum wire (ALW-29S) manufactured by Kulicke and Soffa Bonding Wire (Willow Grove, PA) was used to wedge-bond on 1-mm-thick oxygen-free high conductivity copper substrates supplied by Good Fellow Corporation (Huntingdon, England). The substrates were metallographically polished with Al_2O_3 up to a surface finish of 0.05 μm prior to bonding so that the surface roughness would be similar to that of thin film bond pads. The wedge used was a Kulicke and Soffa part number 4WNV0–2020-W5C-M00 with the geometry, as shown in Fig. 2.

Wedge-bonding was performed with a Kulicke and Soffa 4523D semiautomatic wedge-bonder (60 kHz ultrasonic frequency) with the copper substrate at ambient temperature. The first bond was chosen to be studied. Various parametric conditions were selected for the first bond, and ten bonds were made at each combination of parameters. The normal bonding forces used were low, medium, and high forces of 35 gf, 50 gf, and 65 gf (1 gf = 9.81 mN), respectively, with the bonding time held constant at 30 ms. The ultrasonic powers used were 0 mW, 65 mW, 130 mW, 195 mW, and 260 mW. The second bond was made with fixed parameters of 30 ms bonding time, 35 gf normal bonding force, and an ultrasonic power of 260 mW. An example wedge-wedge wire-bond is shown in top view in Fig. 3.

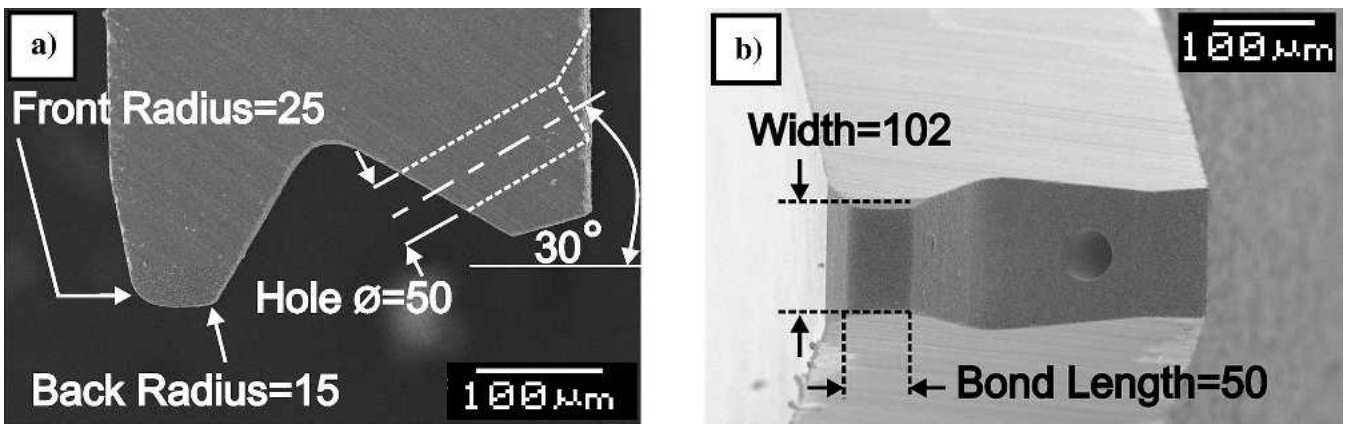

Fig. 2. Wedge geometry used in the study (all dimensions in micrometers): (a) side profile view of the tool and (b) underside of the tool.

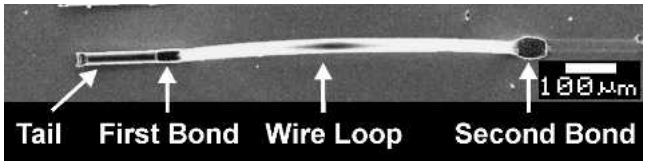

Fig. 3. SEM top view of the wedge-bond showing first bond, second bond, and wire loop.

In order to facilitate more detailed understanding of the bonding mechanisms, bond footprints were examined. Two types of first bond bonding outcomes were obtained, lifted off and sticking, as illustrated in Fig. 4. If the bond was weak, it would result in a lifted-off footprint on the substrate surface. Lifted-off bonds would occur because the force acting on the wire during the following looping step would be greater than the strength of the first bond and would lift the first bond off the substrate. On the other hand, if the bond was sufficiently strong, the first bond would remain on the substrate during the looping step and would subsequently be sheared perpendicular to the wire length with a DAGE 4000 shear tester at a tool height of 3 μm, as shown in Fig. 5, to obtain the sheared footprint.

RESULTS

The bond quality as categorized by a simple sorting model, with lifted-off wedge-bonds as poor quality and bonds remaining on the substrate (sticking) as better quality, is shown in Fig. 6. The morphological features of the bond footprints were examined using SEM and the resulting micrographs including energy-dispersive x-ray (EDX) results are shown in Figs. 7–9. The presence of fractured microwelds in the footprint indicated metallurgical bonding and could be identified by the presence of aluminum left from the wire. Fretted areas as caused

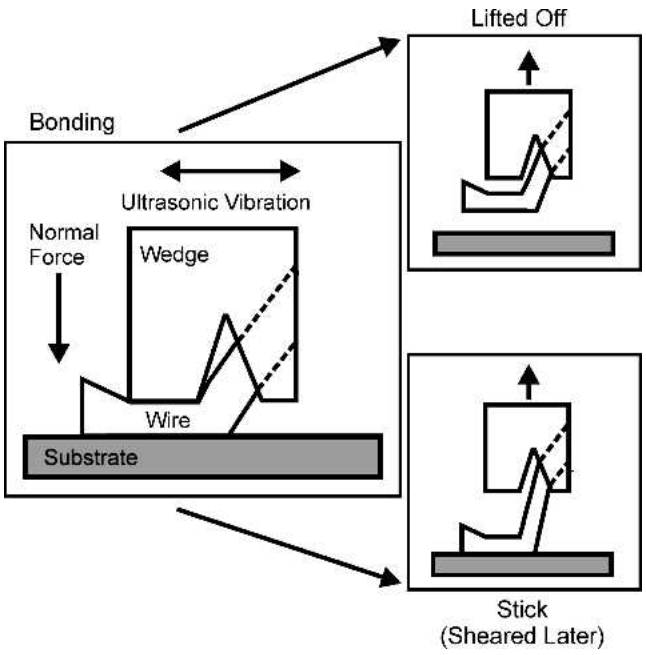

Fig. 4. The two types of bonding outcomes resulting in footprints.

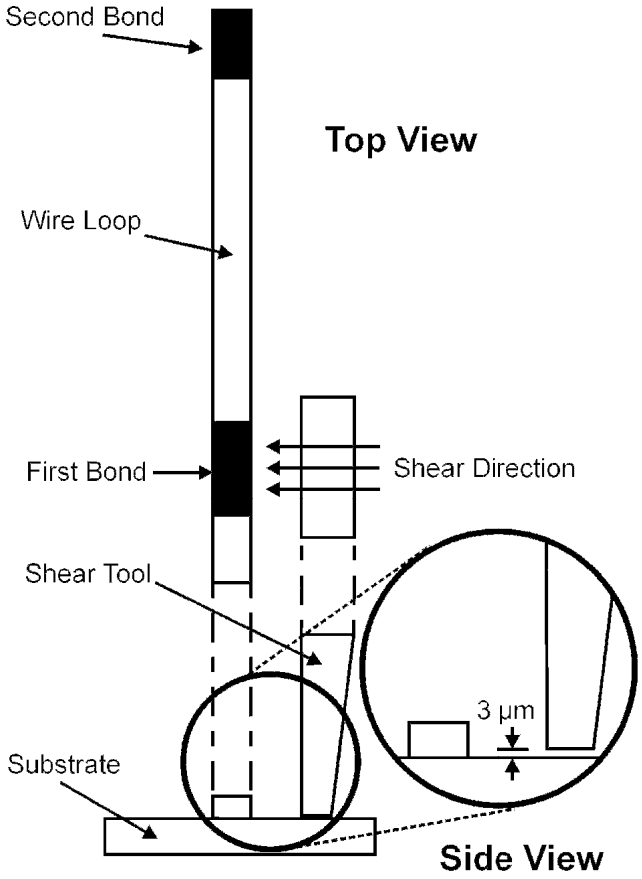

Fig. 5. Schematic of the shearing procedure of a wedge-bond (not to scale).

by interfacial motion from the application of ultrasonic power could also be observed. The fretted areas may indicate areas with material removal but of an insufficient quantity to result in bonding. The widths of the footprints were measured and the results are shown in Fig. 10. No value was determined at the parametric combination 35 gf and 0 mW, as the footprint contrast was too low to allow measurement.

Bonds Made with Low Bonding Force

The effect of varying bonding power at a constant normal bonding force of 35 gf was studied. At 0 mW bonding power, no fretting was observed and all ten bonds (or 100%) lifted off during bonding, as shown in Fig. 6. The absence of fretting was an expected result since there would be no ultrasonic motion when no ultrasonic power was applied. Also, there was no bonding observed, which indicated that compression alone could not result in bonding.

When the bonding power was increased to 65 mW, all ten bonds still lifted off. However, small distinct fretted areas were now observed and were located along an elliptical perimeter slightly inside of the contact ellipse perimeter with no fretting in the center area, as shown by the typical footprint in Fig. 7a. The width of the footprint was about 14 μm (Fig. 10).

With an increase of bonding power to 130 mW, stronger bonding was observed as only one of the bonds lifted off during bonding. Fretted areas and

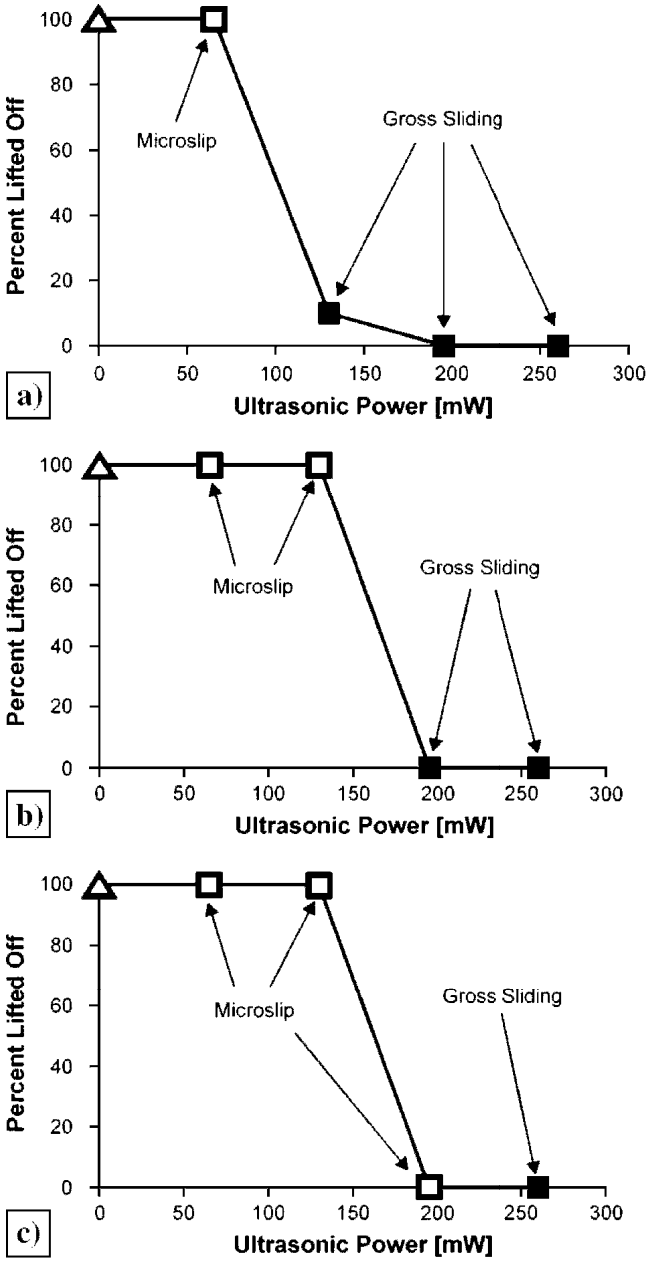

Fig. 6. Percent lifted off versus ultrasonic power for normal bonding forces of (a) 35 gf, (b) 50 gf, and (c) 65 gf. Hollow square symbols indicate microslip condition, while solid square symbols indicate gross sliding. Hollow triangles indicate no bonding. Ten samples per data point.

bonding were clearly visible, as shown in Fig. 7b as a secondary electron image of a sheared bond footprint. Bonded areas, as evidenced by the adherence of aluminum, appear as bright areas in Fig. 7c, which was an aluminum map using EDX analysis of the same area. It is noted here that fretted areas do not necessarily result in bonded areas since the fretted areas in Fig. 7b do not always result in bonded aluminum, as seen in Fig. 7c. From the bond footprint, it can also be seen that the bonding mainly occurred in an elliptical band, with minimal fretting right at the contact periphery and footprint center. The footprint width increased to about 22 μm.

At an increased bonding power of 195 mW, none of the bonds lifted off during bonding. As shown in Fig. 7d, the bonded areas grew to cover the entire footprint area except for an elliptical band at the contact periphery.

At the highest bonding power used, 260 mW, there were no lifted-off bonds. It can be seen in Fig. 7e that the bonding occurred over the entire footprint area except for an elliptical band at the contact periphery. Stronger bonding was evidenced by the large piece of adhering aluminum remaining after shearing. The footprint width was the largest in this group at about 40 μm.

Bonds Made with High Bonding Forces

The effect of bonding power was further investigated with a higher normal bonding force of 50 gf. Without ultrasound, there was no fretting or bonding observed and all ten bonds lifted off (Fig. 6). With a bonding power of 65 mW, there was still no fretting observed, as shown in Fig. 8a, and all bonds lifted off. The absence of fretting was in contrast to the bonds made with the lower bonding force (Fig. 7a). The footprint width was measured to be about 24 μm (Fig. 10) and was significantly larger than the 14 μm measured for the bond made with the lower normal bonding force.

Distinct bonded areas at the two ends of the footprint as well as along the sides at the outer periphery were observed when the bonding power was increased to 130 mW, as shown in Fig. 8b. All ten bonds lifted off, which is in contrast with the bonds made at this same power, but at the lower bonding force, which had only one bond lifted off. It can be observed in Fig. 8b that there existed minimal fretting right at the periphery, but the fretting occurred slightly inside the outer periphery with no fretting in the center area. This absence of fretting in the center area is contrasted with the bonds made at this same power but at lower bonding force (Fig. 7b), which showed fretting at the center area and also had a greater amount of overall fretting.

With a further increase of bonding power to 195 mW, fretted areas were observed across the entire footprint area except for an elliptical band at the periphery, as shown in Fig. 8c. None of the bonds lifted off at this bonding power (Fig. 6) and the footprint width increased to about 35 μm (Fig. 10).

At the highest bonding power used, 260 mW, none of the bonds lifted off during bonding. Figure 8d shows a large piece of aluminum, which evidences strong bonding. It is assumed that fretting had occurred across the entire footprint area with the exception of an elliptical band at the periphery. The width of the footprint increased to about 47 μm.

Finally, the effect of bonding power was investigated with the highest normal bonding force used, 65 gf. The footprints are shown in Fig. 9 and indicate a continuation of the trends observed in the results for the lower normal bonding forces. For example, increased normal bonding force increased

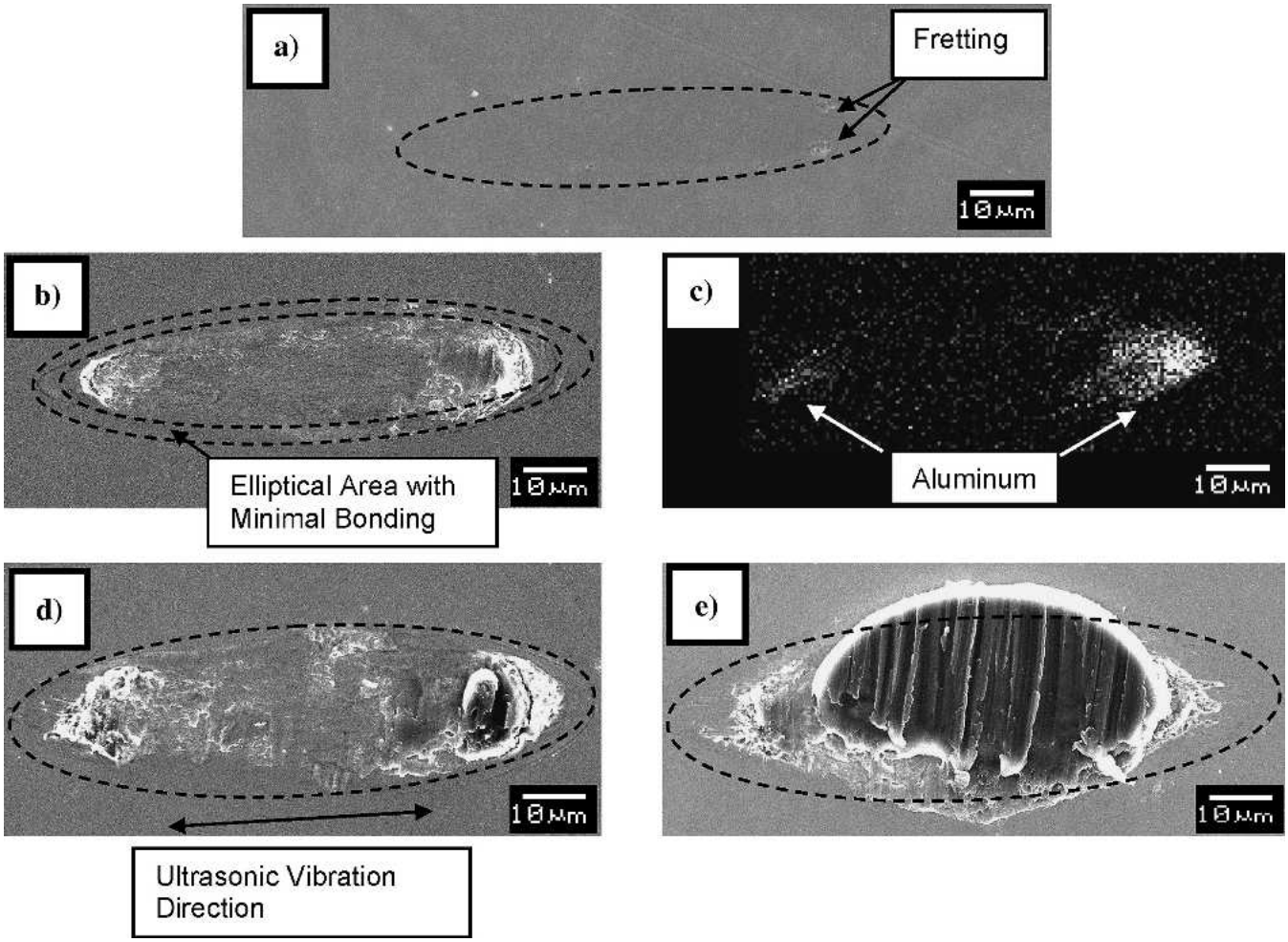

Fig. 7. Bond footprints made with N = 35 gf at various ultrasonic powers: (a) lifted-off bond footprint made at 65 mW, and sheared bond footprints made at (b) 130 mW, (c) EDX aluminum map of the same bond (130 mW) showing aluminum as bright areas, (d) 195 mW, and (e) 260 mW.

the minimum power required for the onset of fretting in the center area from 130 mW, to 195 mW, and to 260 mW for normal bonding forces of 35 gf, 50 gf, and 65 gf, respectively. Similarly, the minimum bonding power required for bond sticking increased from 130 mW for the lowest bonding force to 195 mW for the higher bonding forces. The bond sticking initiation value of 195 mW for the highest normal bonding force used, 65 gf, stands out as an exception because bond sticking was achieved in the microslip regime, whereas in the other parametric combinations, bond sticking was observed only in the gross sliding regime (Fig. 6). The maximum footprint width for a constant ultrasonic bonding power increased with increased normal bonding force (Fig. 10).

DISCUSSION

Bond Footprint Evolution

With an increasing tangential force, a transition from microslip into gross sliding will occur, as predicted by Mindlin's classical microslip theory for perfectly elastic spherical contacts.[1] A similar transition was observed for ultrasonic ball-bonding on copper substrates[5] and also in this study of wedge-bonding even though the wires involved in both cases were plastically deformed.

The evolution of the footprint morphology for wedge-bonding was found to be very similar to that of ball-bonding. However, the contact areas were elliptical compared to the circular contact areas in ball-bonding. It was shown in the results that in wedge-bonding, a transition from microslip into gross sliding still occurred, similar to that reported for ball-bonding. Figure 11 shows such a bond development model for wedge-bonding and illustrates the footprint morphology transitioning from microslip into gross sliding with an increasing tangential force (ultrasonic power). In this generalized model, ball-bonding, as described in Ref. 5, is the special case where the minor and major axes of the ellipse are equal. In Fig. 11, the outer ellipse represents the contact ellipse, the shaded areas indicate the occurrence of relative motion, and the darkness of the shading indicates bonding density (amount of bonding occurring over the area, with darker shading representing higher density). In the following, the results of the tests performed with 50 gf normal bonding force are discussed.

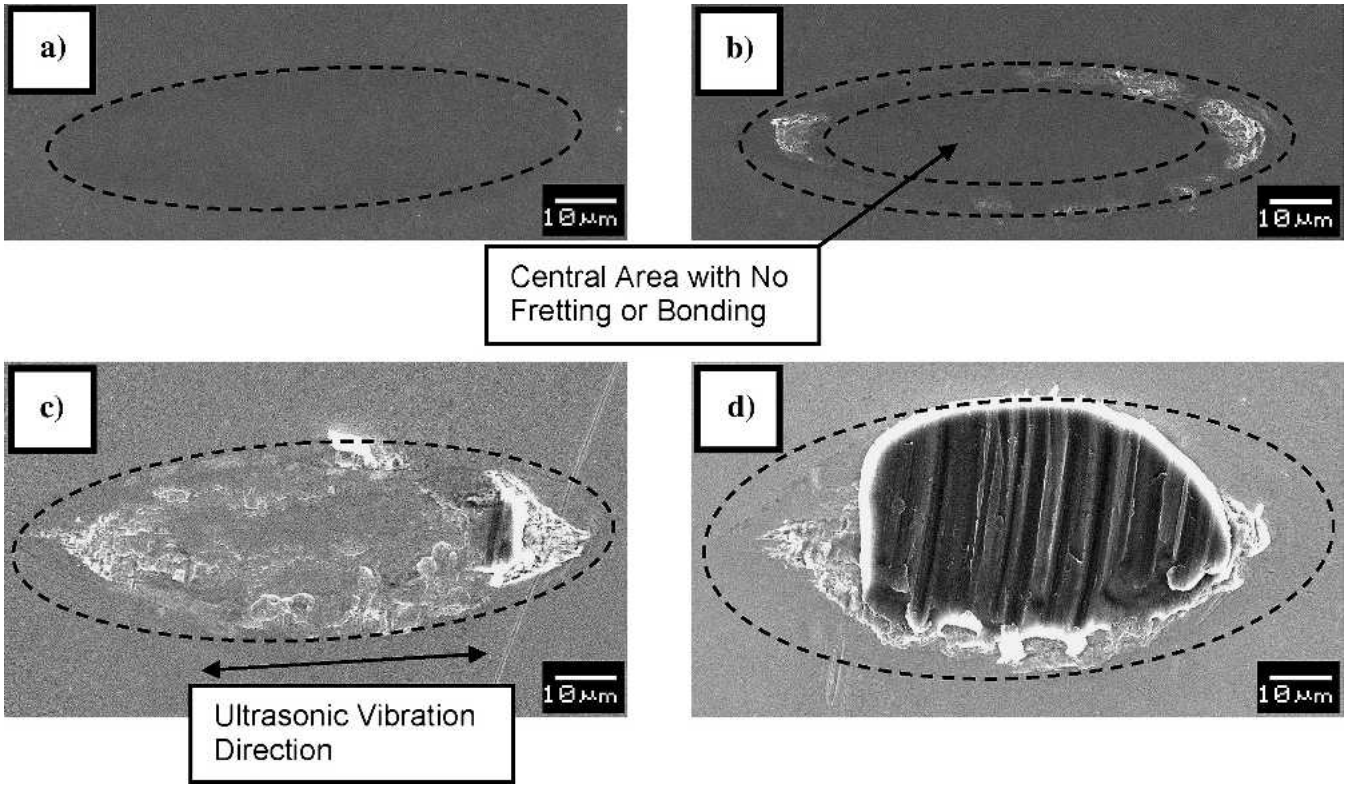

Fig. 8. Bond footprints made with N = 50 gf at various ultrasonic powers. Lifted-off bond footprints made at (a) 65 mW and (b) 130 mW. Sheared bond footprints made at (c) 195 mW and (d) 260 mW.

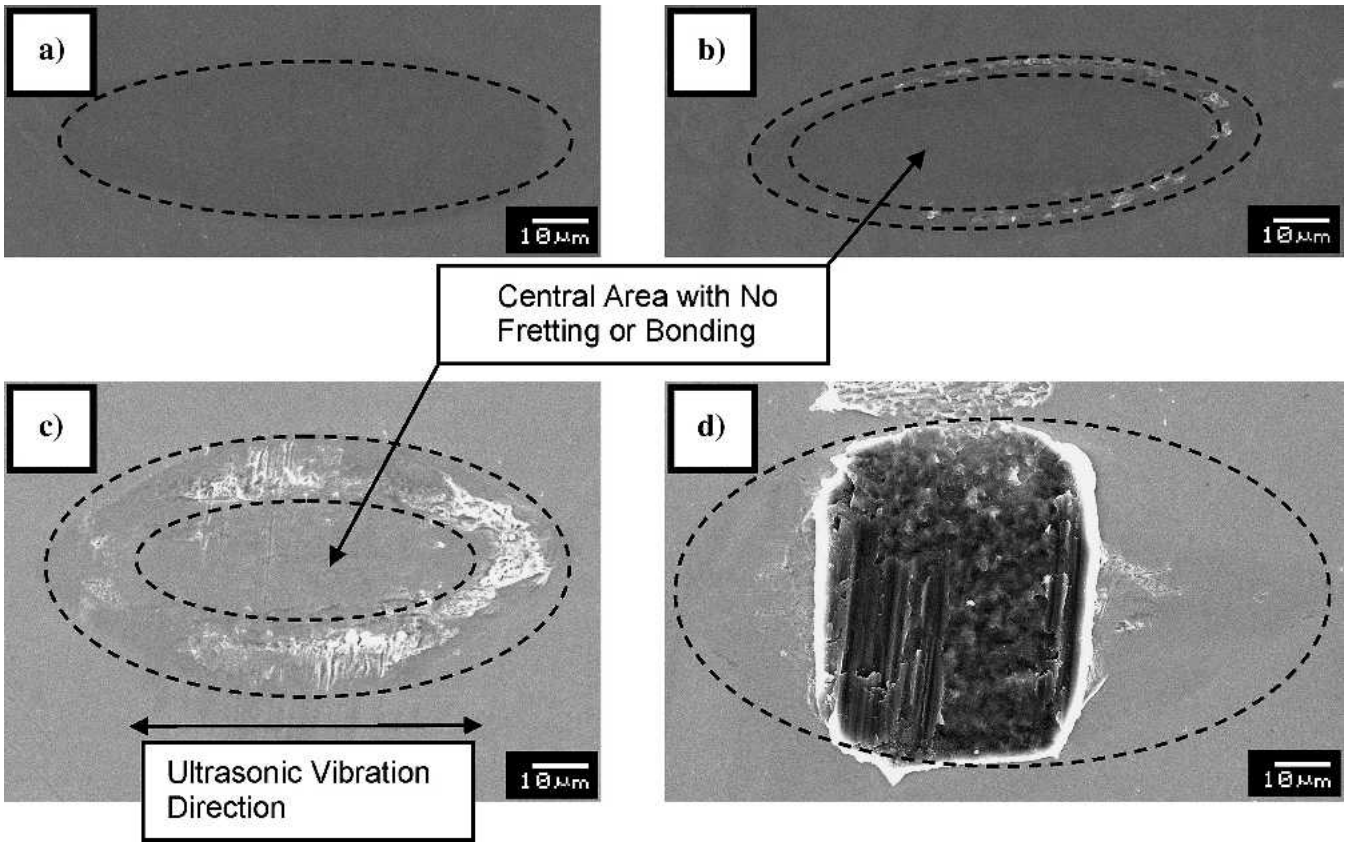

Fig. 9. Bond footprints made with N = 65 gf at various ultrasonic powers. Lifted-off bond footprints made at (a) no ultrasonic energy and (b) 130 mW. Sheared bond footprints made at (c) 195 mW and (d) 260 mW.

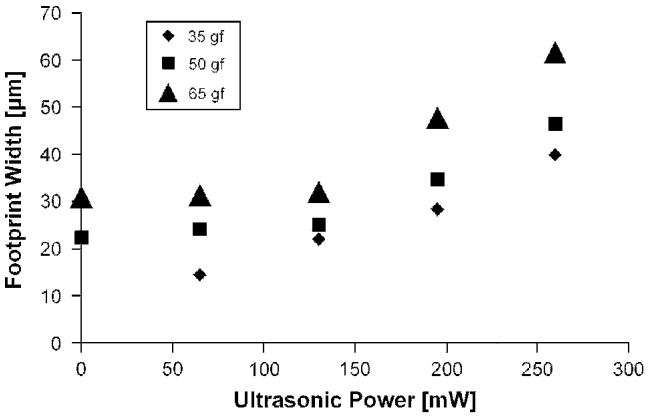

Fig. 10. Footprint width for each representative bond versus ultrasonic power for normal bonding forces of 35 gf, 50 gf, and 65 gf. No value was determined at the parametric combination 35 gf and 0 mW as the footprint contrast was too low to allow measurement.

At low ultrasonic power, microslip will initiate at the periphery and does not reach the center of the footprint, as shown schematically in Fig. 11a. This low power situation is observed for bonding performed at 130 mW in which only an elliptical band of bonding is observed slightly inside of the periphery (Fig. 8b). From the edge of the band out to the contact periphery, there is minimal bonding, which is expected, due to the very low normal stress at the periphery, as shown in Fig. 12a, resulting in the wear of material (as shown by Eq. 1) and subsequent bonding to be much less than in the area closer toward the center of the footprint.

With an increase in ultrasonic bonding power to 195 mW, a change in footprint morphology is observed (Fig. 8c). Fretted and bonded areas grow toward the center of the footprint and now cover the entire area, as shown schematically in Fig. 11b, and indicated a transition into the gross sliding regime. The growth of the microslip elliptical annulus toward the footprint center with increased bonding power is similar to that predicted by Eq. 2, which is for circular contacts. The increase in the footprint width at increased ultrasonic bonding power is attributed to the increased wire deformation due to the increased ultrasonic softening effect at higher bonding power. The elliptical band of minimal fretting/bonding slightly inside of the contact periphery was still observed, as shown in Fig. 8c.

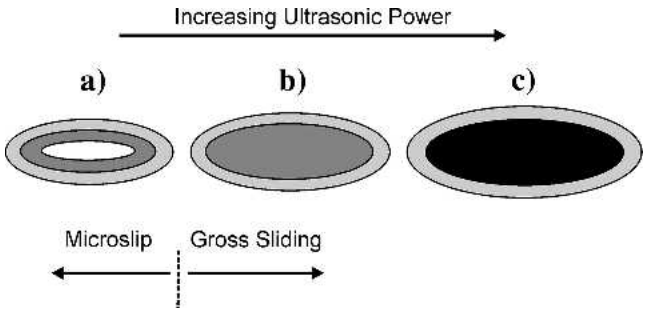

Fig. 11. Schematic illustration of the change in footprint morphology from microslip to gross sliding for increasing ultrasonic power. Shaded areas indicate fretting while bonding density is indicated by the darkness of the shaded area (darker means larger bonding density).

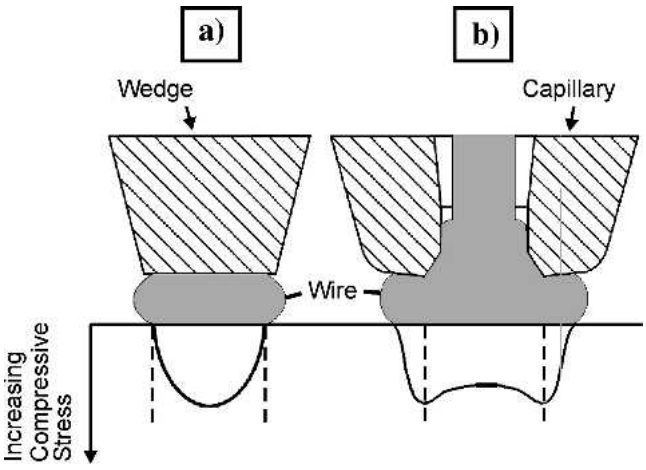

Fig. 12. Suggested normal stress distribution at the wire/substrate interface for (a) wedge-bonding and (b) ball-bonding.

With a further increase of bonding power to 260 mW, the bonding density increased. The higher ultrasonic power increases bonding due to the increased oxide removal, as predicted by Eq. 1. In wedge-bonding, large amounts of bonding were observed in the central area, which is contrasted with the results obtained for a previous ball-bonding study in which the central area remained largely unbonded.[5] This result leads to the conclusion that the lower normal compressive force observed at the center for ball-bonding (Fig. 12b) can cause the reduced center bonding since in wedge-bonding this minimum does not exist and as a result the center is largely bonded.

Winchell and Berg[3] proposed an ultrasonic bonding mechanism for wedge-bonding as a wavelike motion at the bond interface based on their ultrasonic wedge-bonding experiments performed mainly on brittle glass and silicon bonding substrates. They observed what they described as cutting into the substrate at the bond interface, which they proposed could only have been created by wavelike motion. No such cutting was observed in our studies. Further, they discounted the friction or sliding mechanism based on their observation of elliptically shaped footprints with a consistently unbonded central region. The unbonded central region is similar to what is observed in our microslip regime. However, when power is increased and the process transitions into the gross sliding regime, the central region is bonded. Finally, they attributed the bonding to the cleansing of the material surfaces by the wavelike motion at the bond interface and the resulting intimate metal-metal contact. In our study, the cleansing of the surfaces is also shown to be a requirement for metallic bonding; however, it is accomplished by microslip and gross sliding phenomena causing wear of the oxide layer.

Effect of Bonding Force

Figure 6 shows the percent liftoff versus bonding power for varied normal bonding forces, and it is

indicated where the microslip or gross sliding regime was active by the hollow and filled square symbols, respectively. It can be seen that with increased normal bonding force, the microslip to gross sliding transition value shifts toward higher ultrasonic power. This observation agrees with what is predicted by Eq. 2, which states that with increased normal force, tangential force correspondingly needs to be increased in order to achieve gross sliding.

It can also be seen from Fig. 6 that in order to avoid bond liftoffs while increasing normal bonding forces, the ultrasonic power also needs to be increased. This is due to the shifting of the microslip to gross sliding transition value toward higher bonding powers with increasing normal bonding force. In the microslip regime, the outcome was mostly lifted-off bonds. To achieve significant amounts of bonding, and therefore consistent bond sticking, the bonding should be in the gross sliding regime. This observation agrees well with the industrial practice of using an increased ultrasonic power with an increased normal bonding force.[23] The test using the parametric combination of 65 gf and 195 mW stands out as an exception, as bond sticking is achieved while being in the microslip regime close to the edge of the transition line. It is proposed that there can exist a transition area between the microslip and gross sliding regimes where microslip prevails but bond sticking is already possible even at ambient temperature. This transition area is illustrated in Fig. 13. It was observed that bond sticking also coincides with additional ultrasonic deformation of the wire, as evidenced by the footprint width measurements shown in Fig. 10.

Effect of Ultrasonic Energy

Zhou et al.[17] demonstrated in thermosonic gold wire crescent bonding onto gold-plated Kovar that similar amounts of wire deformation achieved with and without ultrasonic energy show different amounts and patterns of bonding. Therefore, the ultrasonic energy may have an additional effect other than increased deformation alone. The additional effect was suggested to be the creation of interfacial relative motion by the application of ultrasonic energy, which is supported by the following discussion.

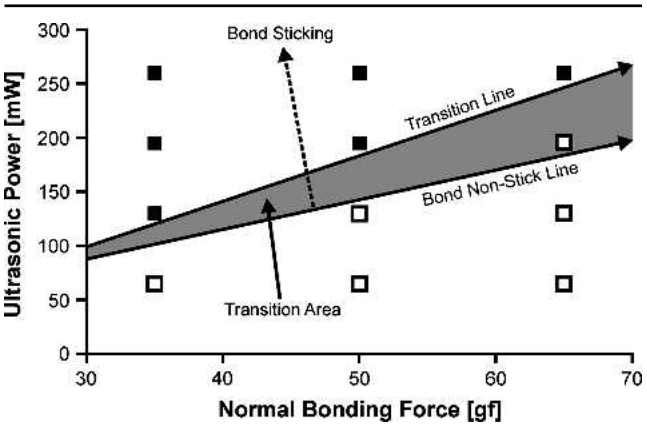

Fig. 13. Postulation of a transition area with bond sticking in the microslip regime, overlaid on the experimental parameter space. Solid square symbols indicate gross sliding condition, while hollow symbols indicate microslip.

In this study, relatively large amounts of interfacial wear (fretting) and bonding were observed for bonds made with relatively low deformation (footprint width of 22 μm) at 35 gf normal bonding force and 130 mW bonding power, as shown in Fig. 7b. When compared to a bonding test made with greater deformation (footprint width of 31 μm) but with no ultrasonic energy (therefore requiring a higher normal bonding force of 65 gf), as shown in Fig. 9a, the effect of ultrasonic energy on bonding is clearly demonstrated. The bonding test made with no ultrasonic energy but having a deformed width about 40% greater than the aforementioned bond showed no bonding. This demonstrates that deformation alone cannot result in bonding for this specific application of bonding carried out in an ambient atmosphere and temperature. Due to the copper oxide, which is relatively ductile,[2] relative motion at the bonding interface created by the application of ultrasonic energy is required for the wearing away of the oxide and subsequent clean metal to metal contact, which results in bonding.

SUMMARY AND CONCLUSIONS

Ultrasonic aluminum wedge-bonds were made on copper substrates at ambient temperature over a range of bonding parameters of ultrasonic power and bonding force. The evolution of the bond footprint morphologies left on the copper substrate was studied in detail with SEM. The major findings from this study are summarized as follows.

- Classical microslip theory is based on circular contacts undergoing elastic deformation. It was shown in this study that a similar transition from microslip to gross sliding occurred with elliptical contacts of a plastically deformed bonding wire on a flat.
- It was found that the evolution of bond footprint morphologies are very similar for ultrasonic gold ball-bonding on copper and ultrasonic aluminum wedge-bonding on copper. A model was developed based on the existing ultrasonic ball-bonding model to explain the general phenomena observed in the evolution of bond footprints during ultrasonic wedge-bonding.
- Relative motion at the bond interface is produced by the ultrasonic vibrations. It exists as either microslip or gross sliding, with the regime being active dependent upon the ultrasonic power and the normal bonding force used. For any given normal bonding force, at lower ultrasonic powers, the bonding is in the microslip regime and with increased power transitions into gross sliding.
- Increased normal bonding force shifts the gross sliding transition toward higher bonding powers, which indicates that for increased normal bonding force, higher power is required to obtain satisfactory bonding.

- It is the interfacial relative motion introduced by the ultrasonic vibration that results in wear of the copper oxide that will lead to intimate metal to metal contact and bonding. In wedge-bonding aluminum wire on copper substrates at room temperature, deformation alone does not result in bonding.
- While increased ultrasonic power grows the microslip region toward the footprint center, it also increases the total size of the footprint due to the increased ultrasonic forces.
- Bond sticking was observed in the microslip regime when relatively high force and ultrasonic parameters were used.
- The center of the contact area is completely bonded at higher ultrasonic power levels in the gross sliding regime. This agrees with what is expected for two sliding bodies. This result verifies that the unbonded circular region observed in a previous ball-bonding study[5] is due to the ringlike geometry of the capillary.

ACKNOWLEDGMENTS

This work has been supported by the Canada Research Chairs Program (www.crc.gc.ca) and the Natural Sciences and Engineering Research Council (NSERC) of Canada (www.nserc.ca).

REFERENCES

1. R.D. Mindlin, *Trans. ASME, Ser. E, J. Appl. Mech.* 16, 259 (1949).
2. G.G. Harman, *Wire Bonding in Microelectronics—Materials, Processes, Reliability, and Yield*, 2nd ed., McGraw-Hill. New York, NY, 1997.
3. V.H. Winchell and H.M. Berg, *IEEE Trans. Components, Hybrids Manufacturing Technol.* CHMT-1, 211 (1978).
4. G.G. Harman and K.O. Leedy, *10th Annual Proc. Reliability Physics* (New York: IEEE, 1972), pp. 49–56.
5. I. Lum, J.P. Jung, and Y. Zhou, *Metall. Mater. Trans. A* 36A, 1279 (2005).
6. C.W. Tan and A.R. Daud, *J. Mater. Sci.: Mater. Electron.* 13, 309 (2002).
7. N. Srikanth et al., *Thin Solid Films* 462–463, 339 (2004).
8. N. Murdeshwar and J.E. Krzanowski, *Metall. Mater. Trans. A* 28A, 2663 (1997).
9. C.L. Yeh and Y.S. Lai, *Microelectron. Reliability* 45, 371 (2005).
10. D. Degryse, B. Vandevelde, and E. Beyne, *IEEE Trans. Components Packaging Technol.* 27, 643 (2004).
11. J.E. Krzanowski, *IEEE Trans. Components Hybrids Manufacturing Technol.* 13, 176 (1990).
12. G.G. Harman and J. Albers, *IEEE Trans. Parts, Hybrids Packaging* PHP-13, 406 (1977).
13. J.E. Krzanowski and N. Murdeshwar, *J. Electron. Mater.* 19, 919 (1990).
14. Y. Takahashi et al., *IEEE Trans. Components Hybrids Manufacturing Technol. Part A* 19, 1996.
15. H.A. Mohamed and J. Washburn, *Welding J.* 54, 302 (1975).
16. B. Langenecker, *IEEE Trans. Sonics Ultrasonics* SU-13 (1966), pp. 1–8.
17. Y. Zhou, X. Li, and N.J. Noolu, *IEEE Trans. Components Packaging Technol.* 28 (4) 810 (2005).
18. M. Mayer (Ph.D. Dissertation 13685, Swiss Federal Institute of Technology (ETH), Zurich, 2002).
19. F. Osterwald, K.D. Lang, and H. Reichl, (Reston, VA: ISHM, 1996), p. 426–431.
20. *ASME Wear Control Handbook*, 1980.
21. M. Mayer and J. Schwizer, *Proc. IMAPS 2002, Proc. SPIE* (Bellingham, WA: The International Society for Optical Engineering, 2002), vol. 4931, pp. 626–631.
22. K.L. Johnson, *Proc. R. Soc. A* 230, 531 (1954).
23. Z.N. Liang, F.G. Kuper, and M.S. Chen, *Microelectron. Reliability* 38, 1287 (1998).